Adjustable intensity-hue-saturation and Brovey transform fusion technique for IKONOS/QuickBird imagery

Te-Ming Tu
Yuh-Chi Lee
Chien-Ping Chang
Ping S. Huang
National Defense University
Department of Electrical Engineering
Chung Cheng Institute of Technology
Taoyuan 33509, Taiwan

Abstract. Among various image fusion methods, intensity-hue-saturation (IHS) and Brovey transforms (BT) can quickly merge huge amounts of IKONOS/QuickBird imagery. However, spectral degradation often appears in the fused images. Moreover, IHS and BT suffer from individual color distortion on saturation compression and saturation stretching, respectively. To balance these two saturation changes during the fusion process, an adjustable IHS-BT approach with spectral adjustment is proposed. Furthermore, to solve the typical bright target recovery (BTR) problems, a simple procedure of dynamic range adjustment (DRA) is also presented. By adopting different DRA techniques, the proposed IHS-BT method is divided into two different fusion approaches: the model of preserving spectral information and the model of enhancing spatial details. Experimental results demonstrate that the proposed combined approaches can achieve significant improvement over other current approaches.
[DOI: 10.1117/1.2124871]

Subject terms: intensity-hue-saturation fusion; Brovey transform; bright target recovery; dynamic range adjustment; spectral adjustment.

Paper 050075R received Jan. 27, 2005; revised manuscript received Apr. 13, 2005; accepted for publication Apr. 14, 2005; published online Nov. 10, 2005.

1 Introduction

Image fusion, also known as image merging or pan sharpening, has become an important issue of remote sensing over the past two decades. With the development and deployment of high-resolution sensors, IKONOS and QuickBird provide spatial resolutions of 4 and 2.4 m for multispectral (MS) imagery, and 1 and 0.6 m for the panchromatic (Pan) data, respectively. Merging MS imagery with the Pan image of higher spatial resolution can increase image interpretive potential as well as improve analytical capabilities.

To date, several methods exist to merge multispectral images of lower resolution with a panchromatic image of higher resolution, particularly for color composites, such as the intensity-hue-saturation (IHS), brovey transform (BT), principal component analysis (PCA), wavelet transform (WT), etc.[1–9] Also, these approaches are already implemented and included in commercial software packages, e.g., PCI Geomatics (PCI Geomatics Enterprises, Incorporated, Richmond Hill, Ontario),[10] RSI ENVI (Research Systems, Incorporated, Bovide, Colorado),[11] and ERDAS IMAGINE (Leica Geosystems, Incorporated, Norcross, GA).[12] However, they normally improve the spatial resolution while the color composite is distorted. Therefore, it is still essential to investigate how to improve the spatial resolution of fused images and simultaneously preserve color information as their original MS images. Most recently, three new and patented fusion techniques[13–15] have been developed for IKONOS and QuickBird imagery. On the other hand, a comparison of four different fusion methods (PCA, modified IHS, wavelet, and Pansharp) for IKONOS data has also been studied.[16] However, there are still more issues that need to be investigated. For the fusion of IKONOS or QuickBird data, the size of a standard scene for an IKONOS image is $11,000 \times 11,000$ pixels, and $27,000 \times 28,000$ pixels for a QuickBird image. Since to merge such a large size of images is computationally intensive, the development of an efficient fusion method becomes nontrivial. To achieve this goal, IHS and BT methods may be feasible for their efficiency and implementation easiness. This work presents a relatively detailed study on these methods and indicates that the color distortion problem arises actually from the saturation changes during the fusion process. In line with theoretical expectations and experimental results, IHS and BT suffer from individual color distortion on saturation compression and saturation stretching, respectively. By combining IHS and BT methods, this work proposes a technique called the adjustable IHS-BT approach, which can simultaneously improve the image resolution and preserve the color as original color composites.

For the 11-bit version of IKONOS/QuickBird imagery, more details can be extracted from scenes that are very dark under shadows or very washed out due to excessive sun reflectance. Because the bright target recovery (BTR)[7,17–21] response is generated when the 11-bit image is scaled down to an 8-bit image, the spatial information loss is significant and not suitable for further applications, e.g., visual interpretation and image mapping purposes. To ease the BTR problem, by combining the square-root contrast stretching

with an unsharpening mask of a high-pass filter, a simple dynamic range adjustment (DRA) technique is utilized to achieve the highest possible spatial details from the original Pan images. The DRA process usually optimizes the most significant portion of the data distribution by sacrificing the least significant portions. By adopting different DRA techniques, the proposed IHS-BT method is divided into two different fusion approaches: the model of preserving spectral information and the model of enhancing spatial details. Their designs are described in this work.

2 New Insight into IHS and BT Image Fusion

2.1 *Image Fusion by Intensity-Hue-Saturation and Brovey Transforms*

IHS and BT are two general and simple fusion methods used for remote sensing images. To reach the goals of image fusion, the IHS method uses three low-resolution multispectral images from distinct bands and transforms them into the IHS color space. Then the intensity component (I) is replaced by the high-resolution Pan image. Next, the new I and previous H and S components are transformed back into the original RGB space. The merged image is a product that synergistically combines the best features from each of those components. However, the direct implementation of the IHS fusion requires numerous multiplication and addition operations for coordinate transformation, making it computationally intensive. To reduce the computation time, a fast version of IHS fusion can be implemented as follows,[5]

$$\begin{bmatrix} \mathrm{R}'_{\mathrm{IHS}} \\ \mathrm{G}'_{\mathrm{IHS}} \\ \mathrm{B}'_{\mathrm{IHS}} \end{bmatrix} = \begin{bmatrix} \mathrm{R} + (\mathrm{Pan} - \mathrm{I}) \\ \mathrm{G} + (\mathrm{Pan} - \mathrm{I}) \\ \mathrm{B} + (\mathrm{Pan} - \mathrm{I}) \end{bmatrix} = \begin{bmatrix} \mathrm{R} + \delta_{\mathrm{IHS}} \\ \mathrm{G} + \delta_{\mathrm{IHS}} \\ \mathrm{B} + \delta_{\mathrm{IHS}} \end{bmatrix}, \tag{1}$$

where $\delta_{\mathrm{IHS}} = \mathrm{Pan} - I$ and the fused image $[R'_{\mathrm{IHS}}, G'_{\mathrm{IHS}}, B'_{\mathrm{IHS}}]^T$ is obtained from the resized original image $[R, G, B]^T$, simply by addition operations.

In contrast to the IHS method, the BT method is a ratio fusion technique that preserves the relative spectral contributions of each pixel, but replaces its overall brightness by the high-resolution panchromatic image. It is operated by

$$\begin{bmatrix} \mathrm{R}'_{\mathrm{BT}} \\ \mathrm{G}'_{\mathrm{BT}} \\ \mathrm{B}'_{\mathrm{BT}} \end{bmatrix} = \frac{\mathrm{Pan}}{\mathrm{I}} \cdot \begin{bmatrix} \mathrm{R} \\ \mathrm{G} \\ \mathrm{B} \end{bmatrix} = \gamma_{\mathrm{BT}} \cdot \begin{bmatrix} \mathrm{R} \\ \mathrm{G} \\ \mathrm{B} \end{bmatrix}, \tag{2}$$

where $\gamma_{\mathrm{BT}} = \frac{\mathrm{Pan}}{I}$.

From Eqs. (1) and (2), it is evident that IHS and BT are indeed simple fusion methods requiring only arithmetical operations without any statistical analysis or filter design. Owing to their efficiency and implementation, either of them can achieve the goal of fast fusion for IKONOS/QuickBird imagery. However, color distortion problems are often produced in the fused images. Hence, originated from the image fusion process, color distortion becomes an important issue for practical applications.

2.2 *Spectral Distortion Originated from IHS and BT Image Fusion*

To discover how the color changes during the image fusion process, Eqs. (1) and (2) are substituted into the following two RGB-IHS conversion models. The first one is a linear transformation[22]:

$$\begin{bmatrix} \mathrm{I} \\ v1 \\ v2 \end{bmatrix} = \begin{bmatrix} 1/3 & 1/3 & 1/3 \\ -\sqrt{2}/6 & -\sqrt{2}/6 & 2\sqrt{2}/6 \\ 1/\sqrt{2} & -1/\sqrt{2} & 0 \end{bmatrix} \begin{bmatrix} \mathrm{R} \\ \mathrm{G} \\ \mathrm{B} \end{bmatrix} \tag{3}$$

and

$$\begin{bmatrix} \mathrm{R} \\ \mathrm{G} \\ \mathrm{B} \end{bmatrix} = \begin{bmatrix} 1 & -1/\sqrt{2} & 1/\sqrt{2} \\ 1 & -1/\sqrt{2} & -1/\sqrt{2} \\ 1 & \sqrt{2} & 0 \end{bmatrix} \begin{bmatrix} \mathrm{I} \\ v1 \\ v2 \end{bmatrix}.$$

Hue (H) and saturation (S) are defined by the internal variables of $v1$ and $v2$, represented by

$$\mathrm{H} = \tan^{-1}\left(\frac{v2}{v1}\right) \quad \text{and} \quad \mathrm{S} = \sqrt{v1^2 + v2^2}. \tag{4}$$

Another model belongs to a nonlinear RGB-IHS conversion system, which rotates the RGB cube until the horizontal plane is parallel to the Maxwell triangle and the vertical axis lies on the gray line of the RGB cube. It is represented by[22]

$$\mathrm{I} = (\mathrm{R} + \mathrm{G} + \mathrm{B})/3, \tag{5}$$

$$\mathrm{H} = \begin{cases} \cos^{-1}(\varphi), & \text{if } \mathrm{G} \geqslant \mathrm{R} \\ 2\pi - \cos^{-1}(\varphi), & \text{if } \mathrm{G} \leqslant \mathrm{R} \end{cases},$$
$$\varphi = \frac{(2\mathrm{B} - \mathrm{G} - \mathrm{R})/2}{[(\mathrm{B} - \mathrm{G})^2 + (\mathrm{B} - \mathrm{R})(\mathrm{G} - \mathrm{R})]^{\frac{1}{2}}}, \tag{6}$$

and

$$\mathrm{S} = 1 - \frac{3\min(\mathrm{R},\mathrm{G},\mathrm{B})}{\mathrm{R} + \mathrm{G} + \mathrm{B}} = \frac{\mathrm{I} - a}{\mathrm{I}}, \tag{7}$$

where

$$a = \min(\mathrm{R},\mathrm{G},\mathrm{B}).$$

By substituting Eq. (1) into the linear RGB-IHS conversion model of Eq. (3), we get

$$\begin{bmatrix} R'_{IHS} \\ G'_{IHS} \\ B'_{IHS} \end{bmatrix} = \begin{bmatrix} R + \delta_{IHS} \\ G + \delta_{IHS} \\ B + \delta_{IHS} \end{bmatrix} = \begin{bmatrix} Pan \\ Pan \\ Pan \end{bmatrix} + \begin{bmatrix} -1/\sqrt{2} & 1/\sqrt{2} \\ -1/\sqrt{2} & -1/\sqrt{2} \\ \sqrt{2} & 0 \end{bmatrix} \begin{bmatrix} v1 \\ v2 \end{bmatrix}. \tag{8}$$

From Eq. (8), it is important to recognize that both H and S defined by Eq. (4) are preserved after fusion; only the intensity component I has been replaced by Pan.

On the other hand, by substituting Eq. (1) into the nonlinear RGB-IHS conversion system of Eqs. (5), (6), and (7), we have

$$I' = [(R + \delta_{IHS}) + (G + \delta_{IHS}) + (B + \delta_{IHS})]/3 = I + \delta_{IHS} = Pan, \tag{9}$$

$$\varphi' = \frac{[2(B + \delta_{IHS}) - (G + \delta_{IHS}) - (R + \delta_{IHS})]/2}{\{[(B + \delta_{IHS}) - (G + \delta_{IHS})]^2 + [(B + \delta_{IHS}) - (R + \delta_{IHS})][(G + \delta_{IHS}) - (R + \delta_{IHS})]\}^{\frac{1}{2}}} = \frac{(2B - G - R)/2}{[(B - G)^2 + (B - R)(G - R)]^{\frac{1}{2}}} = \varphi, \tag{10}$$

$$S' = 1 - \frac{3\min(R + \delta_{IHS}, G + \delta_{IHS}, B + \delta_{IHS})}{R + G + B + 3\delta_{IHS}} = \frac{I' - a'}{I'} = \frac{I - a}{Pan}; \quad a' = \min(R', G', B') = a + \delta_{IHS}. \tag{11}$$

To divide S' in Eq. (11) by S in Eq. (7), an important relationship can be obtained by

$$\frac{S'}{S} = \frac{I}{Pan} \text{ or } I \cdot S = Pan \cdot S' = \text{constant}. \tag{12}$$

By observing Eqs. (9)–(12), for IHS image fusion in the nonlinear color model, the product of saturation and intensity equals a constant value and the hue value is unchanged. The saturation value of a pixel is inversely proportional to its intensity value. More precisely, the saturation value is expanded and stretched ($S' > S$) if the Pan value is less than the I value, while the saturation value is compressed ($S' < S$) if the Pan value is larger than the I value.

To evaluate the effect of color distortion resulted from the BT method and follow the procedures for IHS fusion, Eq. (2) can also be substituted into Eqs. (3), (5), (6), and (7). The obtained results of Eq. (3) are represented by

$$\begin{bmatrix} R'_{BT} \\ G'_{BT} \\ B'_{BT} \end{bmatrix} = \gamma_{BT} \cdot \begin{bmatrix} R \\ G \\ B \end{bmatrix} = \begin{bmatrix} Pan \\ Pan \\ Pan \end{bmatrix} + \begin{bmatrix} -1/\sqrt{2} & 1/\sqrt{2} \\ -1/\sqrt{2} & -1/\sqrt{2} \\ \sqrt{2} & 0 \end{bmatrix} \times \begin{bmatrix} \gamma_{BT} \cdot v1 \\ \gamma_{BT} \cdot v2 \end{bmatrix}. \tag{13}$$

From the definition of Eq. (4), the hue value of the fused image is the same as its corresponding value of the original RGB image, but the saturation value has been altered. That is,

$$H' = \tan^{-1}\left(\frac{\gamma_{BT} \cdot v2}{\gamma_{BT} \cdot v1}\right) = H, \tag{14}$$

$$S' = [(\gamma_{BT} \cdot v1)^2 + (\gamma_{BT} \cdot v2)^2]^{\frac{1}{2}} = \gamma_{BT} \cdot \sqrt{v1^2 + v2^2} = \frac{Pan}{I} \cdot S. \tag{15}$$

Meanwhile, the results obtained from Eqs. (5), (6), and (7) are given as follows,

$$I' = (\gamma_{BT} \cdot R + \gamma_{BT} \cdot G + \gamma_{BT} \cdot B)/3 = \gamma_{BT} \cdot I = Pan, \tag{16}$$

$$\varphi' = \frac{(2B'_{BT} - G'_{BT} - R'_{BT})/2}{[(B'_{BT} - G'_{BT})^2 + (B'_{BT} - R'_{BT})(G'_{BT} - R'_{BT})]^{\frac{1}{2}}} = \frac{\gamma_{BT} \cdot (2B - G - R)/2}{\gamma_{BT} \cdot [(B - G)^2 + (B - R)(G - R)]^{\frac{1}{2}}} = \varphi, \tag{17}$$

$$S' = 1 - \frac{3\min(R'_{BT}, G'_{BT}, B'_{BT})}{R'_{BT} + G'_{BT} + B'_{BT}} = 1 - \frac{\gamma_{BT} \cdot \min(R, G, B)}{\gamma_{BT} \cdot (R + G + B)/3} = S. \tag{18}$$

Equations (16), (17), and (18) reveal an interesting fact that both hue and saturation values of the fused image equal their corresponding values in the original RGB image. This consequence is the same as the IHS method in Eq. (8). However, they appear in two different RGB-IHS conversion systems. Furthermore, by referring to Eqs. (14) and (15), the hue value of the fused image is the same as its corresponding value of the original RGB image, but the saturation value has been altered. In contrast to the IHS method in Eq. (12), where the saturation value is stretched when the Pan value is larger than the I value, the result in Eq. (15) shows that the saturation value is compressed when the Pan value is less than the I value. This is the main difference between IHS and BT in color distortion problems.

It is found from experimental results that both IHS and BT maintain the same spatial resolution as the Pan image, but distort the saturation information. Hence, the IHS

method works properly under the nonlinear RGB-IHS conversion system, while the BT method works in the linear RGB-IHS conversion system. This can also be concluded from the previous comparisons between IHS and BT.

3 Problems and Solutions

3.1 *Spectral Mismatch between the Pan and MS Bands*

Apart from the color distortion problems, another issue of IHS/BT image fusion for IKONOS/QuickBird imagery arises from the changes of the panchromatic spectral range. As we can see from Fig. 1, for the spectral responses of IKONOS/QuickBird imagery, the wavelength of IKONOS and QuickBird panchromatic images is ranging from visible to near-infrared bands. By observing the real IKONOS/QuickBird images, the digital number (DN) values of I in most land covers such as buildings, roads, and soil regions, are slightly larger or smaller than their corresponding values in Pan. Nevertheless, this situation is not sufficient to affect the quality of image fusion. Considering the green vegetation regions, however, their DN values in Pan are far larger than those in I because of the influence of near-infrared contents. This will produce large δ_{IHS} and γ_{BT} values and result in significant color distortion in green vegetation regions of the fused image. Using the IHS method, those green vegetation regions are forced to undergo various degrees of saturation compressing, and this situation is contrary to the situation of the BT approach which appears as saturation stretching.

To significantly reduce the degree of color distortion, an appropriate adjustment strategy is needed to lower the δ_{IHS} and γ_{BT} values in the process of IHS/BT fusion. To do this, a generalized IHS (GIHS) method[8] has been proposed to cope with this problem for IKONOS images. It is represented by

$$\begin{bmatrix} \mathrm{R}'_{\mathrm{GIHS}} \\ \mathrm{G}'_{\mathrm{GIHS}} \\ \mathrm{B}'_{\mathrm{GIHS}} \\ \mathrm{NIR}'_{\mathrm{GIHS}} \end{bmatrix} = \begin{bmatrix} \mathrm{R} + \delta_{\mathrm{GIHS}} \\ \mathrm{G} + \delta_{\mathrm{GIHS}} \\ \mathrm{B} + \delta_{\mathrm{GIHS}} \\ \mathrm{NIR} + \delta_{\mathrm{GIHS}} \end{bmatrix}, \tag{19}$$

where $\delta_{\mathrm{GIHS}} = \mathrm{Pan}\text{-}I' = \mathrm{Pan}\text{-}R+G+B+NIR/4$ and $I' = R+G+B+NIR/4$. In Eq. (19), the saturation compression can be efficiently mitigated by introducing the NIR band into I. This is due to the vegetation regions in the NIR band revealing relatively high reflectance, and low reflectance is displayed in RGB bands. It is easy to prove that I' is larger than I, so that the goal of lowering the δ_{IHS} value has been achieved. To further consider the spectral mismatch between the Pan and MS bands, a simple spectral adjustment IHS (SA-IHS) method was proposed in Ref. 8. That is, to use the term of $I'' = \frac{R+0.75*G+0.25*B+NIR}{3}$ to replace I' in Eq. (19). The weighting parameters 0.75 and 0.25 are used to lessen two spectral mismatches in Fig. 1(a), where the green band is not fully covered by the spectral response of the Pan band and most of the blue band falls outside the 3-dB level of the Pan band. Experimental results demonstrate that the SA-IHS method can achieve the least color distortion to the IKONOS image fusion.

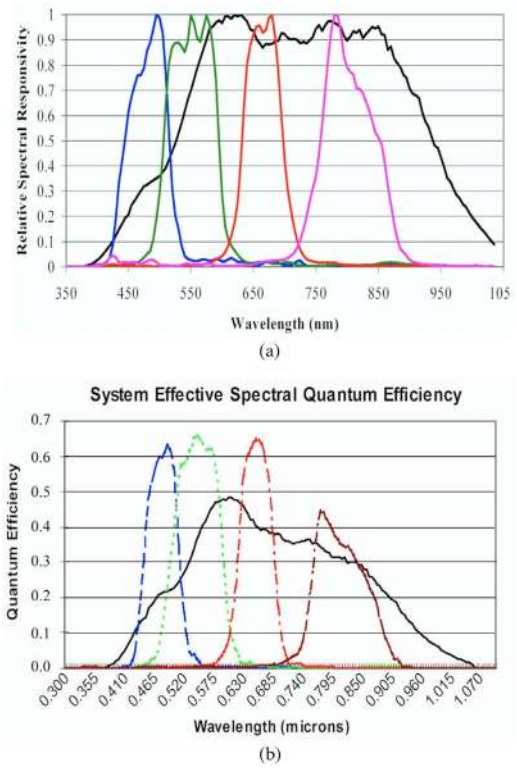

Fig. 1 The spectral responses of (a) IKONOS imagery and (b) QuickBird imagery.

By referring to the modified schemes of the IHS method, the generalized and spectral adjustment BT approaches can be directly obtained by

$$\begin{bmatrix} \mathrm{R}'_{\mathrm{GBT}} \\ \mathrm{G}'_{\mathrm{GBT}} \\ \mathrm{B}'_{\mathrm{GBT}} \\ \mathrm{NIR}_{\mathrm{GBT}} \end{bmatrix} = \frac{\mathrm{Pan}}{\mathrm{I}'} \cdot \begin{bmatrix} \mathrm{R} \\ \mathrm{G} \\ \mathrm{B} \\ \mathrm{NIR} \end{bmatrix}$$

and

$$\begin{bmatrix} \mathrm{R}'_{\mathrm{SA\text{-}BT}} \\ \mathrm{G}'_{\mathrm{SA\text{-}BT}} \\ \mathrm{B}'_{\mathrm{SA\text{-}BT}} \\ \mathrm{NIR}'_{\mathrm{SA\text{-}BT}} \end{bmatrix} = \frac{\mathrm{Pan}}{\mathrm{I}''} \cdot \begin{bmatrix} \mathrm{R} \\ \mathrm{G} \\ \mathrm{B} \\ \mathrm{NIR} \end{bmatrix}, \tag{20}$$

where the definitions of I' and I'' are the same as those values given for the GIHS and SA-IHS methods. Based on earlier discussion, we would believe that both the generalized BT (GBT) and spectral adjustment BT (SA-BT) can effectively remedy the problems of saturation stretch that appeared from the original BT method.

It is important to note that those two weighting parameters, 0.75 and 0.25, in I'' are the optimal values determined from 92 IKONOS images covering different areas,[8] and they should be reconsidered for the QuickBird image fusion. By referring to Fig. 1, those two figures are indeed similar after the spectral response of the QuickBird image is adjusted to the scale of the IKONOS image. Therefore,

we believe that those two weighting parameters, 0.75 and 0.25, are also suitable to represent the reflectance of spectral response for QuickBird images.

3.2 *Balancing the Color Distortion in IHS with BT*

Let us return to the color distortion problems in IHS and BT image fusion. Equations (12) and (15) show that the color distortion in IHS is contrary to that in the BT method. On green vegetation regions of the fused image, the IHS technique generates significant saturation compression, while the BT method suffers from saturation stretch on the same regions. Motivated from the idea that saturation compression is contrary to saturation stretch, we propose that combining IHS with BT to balance various saturation changes may reduce the saturation distortion problems. This work presents an adjustable IHS-BT approach represented by

$$\begin{bmatrix} \mathrm{R}'_{\mathrm{IHS\text{-}BT}} \\ \mathrm{G}'_{\mathrm{IHS\text{-}BT}} \\ \mathrm{B}'_{\mathrm{IHS\text{-}BT}} \\ \mathrm{NIR}'_{\mathrm{IHS\text{-}BT}} \end{bmatrix} = \frac{\mathrm{Pan}}{\mathrm{I}+k\cdot\delta_{\mathrm{IHS}}} \begin{bmatrix} \mathrm{R}+k\cdot\delta_{\mathrm{IHS}} \\ \mathrm{G}+k\cdot\delta_{\mathrm{IHS}} \\ \mathrm{B}+k\cdot\delta_{\mathrm{IHS}} \\ \mathrm{NIR}+k\cdot\delta_{\mathrm{IHS}} \end{bmatrix} = \frac{\mathrm{Pan}}{\mathrm{I}+k\cdot(\mathrm{Pan}-\mathrm{I})} \cdot \begin{bmatrix} \mathrm{R}+k\cdot(\mathrm{Pan}-\mathrm{I}) \\ \mathrm{G}+k\cdot(\mathrm{Pan}-\mathrm{I}) \\ \mathrm{B}+k\cdot(\mathrm{Pan}-\mathrm{I}) \\ \mathrm{NIR}+k\cdot(\mathrm{Pan}-\mathrm{I}) \end{bmatrix}, \tag{21}$$

where k is a weighting parameter used to control the degree of saturation stretch/compression in the fused image, and $0<k<1$. When $k=0$, IHS-BT is identical to BT and IHS-BT becomes the IHS method while $k=1$. For the purpose of saturation balance, $k=0.5$ is a good and reasonable choice.

To verify if the saturation of the fused image has been balanced, $[R'_{\mathrm{IHS\text{-}BT}}, G'_{\mathrm{IHS\text{-}BT}}, B'_{\mathrm{IHS\text{-}BT}}]^T$ in Eq. (21) is substituted into Eqs. (3), (5), (6), and (7). From Eq. (3), we get

$$\begin{bmatrix} \mathrm{R}'_{\mathrm{IHS\text{-}BT}} \\ \mathrm{G}'_{\mathrm{IHS\text{-}BT}} \\ \mathrm{B}'_{\mathrm{IHS\text{-}BT}} \end{bmatrix} = \begin{bmatrix} \mathrm{Pan} \\ \mathrm{Pan} \\ \mathrm{Pan} \end{bmatrix} + \begin{bmatrix} -1/\sqrt{2} & 1/\sqrt{2} \\ -1/\sqrt{2} & -1/\sqrt{2} \\ \sqrt{2} & 0 \end{bmatrix} \begin{bmatrix} \gamma_{\mathrm{IHS\text{-}BT}}\cdot\nu 1 \\ \gamma_{\mathrm{IHS\text{-}BT}}\cdot\nu 2 \end{bmatrix}, \tag{22}$$

where $\gamma_{\mathrm{IHS\text{-}BT}}=\mathrm{Pan}/I+k\cdot\delta_{\mathrm{IHS}}=\mathrm{Pan}/k\cdot\mathrm{Pan}+(1-k)\cdot\mathrm{I}$. Accordingly, the values of hue and saturation can be given by

$$\mathrm{H}' = \tan^{-1}\left(\frac{\gamma_{\mathrm{IHS\text{-}BT}}\cdot\nu 2}{\gamma_{\mathrm{IHS\text{-}BT}}\nu 1}\right) = \mathrm{H}, \tag{23}$$

$$\mathrm{S}' = [(\gamma_{\mathrm{IHS\text{-}BT}}\cdot\nu 1)^2 + (\gamma_{\mathrm{IHS\text{-}BT}}\cdot\nu 2)^2]^{\frac{1}{2}} = \gamma_{\mathrm{IHS\text{-}BT}}\cdot\mathrm{S} = \frac{\mathrm{Pan}}{k\cdot\mathrm{Pan}+(1-k)\cdot\mathrm{I}}\cdot\mathrm{S}. \tag{24}$$

Correspondingly, from Eqs. (5), (6), and (7), we have

$$\mathrm{I}' = (\mathrm{R}'_{\mathrm{IHS\text{-}BT}} + \mathrm{G}'_{\mathrm{IHS\text{-}BT}} + \mathrm{B}'_{\mathrm{IHS\text{-}BT}})/3 = \mathrm{Pan}, \tag{25}$$

$$\varphi' = \frac{(2\mathrm{B}'_{\mathrm{IHS\text{-}BT}} - \mathrm{G}'_{\mathrm{IHS\text{-}BT}} - \mathrm{R}'_{\mathrm{IHS\text{-}BT}})/2}{[(\mathrm{B}'_{\mathrm{IHS\text{-}BT}} - \mathrm{G}'_{\mathrm{IHS\text{-}BT}})^2 + (B'_{\mathrm{IHS\text{-}BT}} - \mathrm{R}'_{\mathrm{IHS\text{-}BT}})(\mathrm{G}'_{\mathrm{IHS\text{-}BT}} - \mathrm{R}'_{\mathrm{IHS\text{-}BT}})]^{\frac{1}{2}}} = \varphi, \tag{26}$$

$$\mathrm{S}' = 1 - \frac{3\min(\mathrm{R}'_{\mathrm{IHS\text{-}BT}}, \mathrm{G}'_{\mathrm{IHS\text{-}BT}}, \mathrm{B}'_{\mathrm{IHS\text{-}BT}})}{\mathrm{R}'_{\mathrm{IHS\text{-}BT}} + \mathrm{G}'_{\mathrm{IHS\text{-}BT}} + \mathrm{B}'_{\mathrm{IHS\text{-}BT}}} = \left(\frac{\mathrm{I}}{\mathrm{I}+k\cdot\delta_{\mathrm{IHS}}}\right)\cdot\mathrm{S} = \frac{\mathrm{I}}{k\cdot\mathrm{Pan}+(1-k)\cdot\mathrm{I}}\cdot\mathrm{S}. \tag{27}$$

Based on the derived Eqs. (22)–(27), the proposed adjustable IHS-BT approach demonstrates that the spatial resolution and the hue value are the same as those accomplished by the IHS/BT methods, only the saturation component is changed in both IHS spaces. To further investigate the perceived saturation properties achieved by IHS/BT methods, we let $k=0.5$. Then S' in Eqs. (24) and (27) can be obtained as

$$\mathrm{S}'_{\mathrm{IHS\text{-}BT}} = \frac{\mathrm{Pan}}{0.5\cdot\mathrm{Pan}+0.5\cdot\mathrm{I}}\cdot\mathrm{S} = \frac{2\cdot\mathrm{Pan}}{\mathrm{Pan}+\mathrm{I}}\cdot\mathrm{S}, \tag{28}$$

$$\text{and } \mathrm{S}'_{\mathrm{IHS\text{-}BT}} = \frac{\mathrm{I}}{0.5\cdot\mathrm{Pan}+0.5\cdot\mathrm{I}}\cdot\mathrm{S} = \frac{2\cdot\mathrm{I}}{\mathrm{Pan}+\mathrm{I}}\cdot\mathrm{S}. \tag{29}$$

For the purpose of comparison, S' in Eqs. (12) and (15) are rewritten and represented by

$$\mathrm{S}'_{\mathrm{BT}} = \frac{\mathrm{Pan}}{\mathrm{I}}\cdot\mathrm{S} \quad (\text{from BT}), \tag{30}$$

$$\text{and } \mathrm{S}'_{\mathrm{IHS}} = \frac{\mathrm{I}}{\mathrm{Pan}}\cdot\mathrm{S} \quad (\text{from IHS}). \tag{31}$$

Since the DN values of Pan are far larger than those of I, only green vegetation regions suffer from the significant problem of saturation compression/stretch in IKONOS/QuickBird images. It is easy to prove that $S'_{\mathrm{IHS\text{-}BT}}$ in Eq. (28) is less than S'_{BT} in Eq. (30), while $S'_{\mathrm{IHS\text{-}BT}}$ in Eq. (29) is larger than S'_{IHS} in Eq. (31). Compared to either of S'_{BT} and S'_{IHS}, $S'_{\mathrm{IHS\text{-}BT}}$ is closer to the original value of S. That is, the

proposed adjustable IHS-BT approach can really reduce the saturation changes produced by BT or IHS after the image fusion.

Without loss of generality, again, the adjustable IHS-BT approach of Eq. (21) can be directly extended to its generalized and spectral adjustment versions. They are

$$\begin{bmatrix} R'_{GIHS\text{-}BT} \\ G'_{GIHS\text{-}BT} \\ B'_{GIHS\text{-}BT} \\ NIR'_{GIHS\text{-}BT} \end{bmatrix} = \frac{Pan}{I' + k \cdot (Pan - I')} \cdot \begin{bmatrix} R + k \cdot (Pan - I') \\ G + k \cdot (Pan - I') \\ B + k \cdot (Pan - I') \\ NIR + k \cdot (Pan - I') \end{bmatrix}, \quad (32)$$

and

$$\begin{bmatrix} R'_{SA\text{-}IHS\text{-}BT} \\ G'_{SA\text{-}IHS\text{-}BT} \\ B'_{SA\text{-}IHS\text{-}BT} \\ NIR'_{SA\text{-}IHS\text{-}BT} \end{bmatrix} = \frac{Pan}{I'' + k \cdot (Pan - I'')} \cdot \begin{bmatrix} R + k \cdot (Pan - I'') \\ G + k \cdot (Pan - I'') \\ B + k \cdot (Pan - I'') \\ NIR + k \cdot (Pan - I'') \end{bmatrix}. \quad (33)$$

To verify the efficacy of the proposed technique given in Eqs. (21), (32), and (33), real IKONOS/QuickBird images are used in the experiments carried out in the following section.

3.3 *Implementation Considerations*

Both IKONOS and QuickBird offer 11-bit Pan and MS data. Technically, this means that more details can be extracted from scenes that are very dark under shadows or very washed out due to excessive sun reflectance. By merging those 11-bit format data, however, the fused images usually provide low contrast, and their overall average brightness level is too dark to be accepted. On the other hand, the data output of many digital imaging devices is usually 8 bits. To scale the 11-bit fused image down to an 8-bit image by an improper DRA induces a BTR response that results in the loss of spatial information.[7,17–21]

The critical issue of image fusion focuses on how to produce a fused imagery of high quality. To preserve spectral information, the scaled 8-bit Pan and MS imagery should try to retain the spectral information of their original 11-bit versions as much as possible. The selected DRA process is usually used to optimize the most significant portion of the data histogram by sacrificing the least significant parts. Under this criterion, a minimum/maximum percent cutoff approach followed by a linear stretching can be used to preserve most spectral/spatial information of the original 11-bit MS/Pan imagery. By doing that, however, the BTR responses appear in white roofs, and the spatial details under the shadow of buildings are lost. The losses are generated by cutting the two ends of the data histogram.

To solve the BTR problems, the dynamic range of the Pan image should be effectively compressed. The fused imagery should offer the highest possible spatial information content and still preserve good spectral information quality. To fulfill this requirement, a simple technique of square root stretching followed by an unsharpening mask of a high-pass filter is used to tackle the BTR problems. Based on the previous discussions, to produce a fused imagery of high quality, a suggested classification/visualization oriented procedure is summarized in the following steps.

1. Upsample (or resize) the MS (R, G, B, and NIR bands) imagery of low spatial resolution to the size of the Pan image of high spatial resolution.
2. Part 1: For preserving spectral information, a minimum/maximum 0.5 to 2 % cutoff is applied to adjust the dynamic range of Pan/MS images, followed by a linear stretching to scale the 11-bit image down to an 8-bit image.
   Part 2: To resolve the BTR problem for image interpretation or mapping, the 11-bit Pan image must be preprocessed by using square root stretching to compress the dynamic range. To increase the contrast of spatial details, an unsharpening mask filter is further performed at the 8-bit Pan image.
3. Depending on the purpose of a given application, the output images generated from parts 1 and 2 in step 2 are substituted into Eq. (33).

The suggested procedures have been implemented into a Windows-based program consisting of two windows, the Scroll window and the Main Image window, respectively. The input RGB image is displayed in the Scroll window at subsampled resolution. The indicator of the Main Image window appears as a box within the Scroll window and outlines the area that is displayed in full resolution in the Main Image window. To simplify the procedures and choose a good balancing parameter k, the program only initially reads and fuses the associated images within the Main Image window. After k is determined, the fusion is then performed at the entire image. According to various demands, the fused images for the small area and the entire image displayed in the Main Image window can be individually selected and stored.

4 Experimental Results

Three experiments are conducted in this section. The first two experiments use real IKONOS and QuickBird images to evaluate nine fusion methods, respectively. Those nine methods are the original versions of IHS, BT, and IHS-BT, the generalized versions of GIHS, GBT, and GIHS-BT, and the spectral adjustment versions of SA-IHS, SA-BT, and SA-IHS-BT. In the third experiment, a QuickBird image is adopted to illustrate that the proposed procedure can effectively reduce the BTR response and provide a good visualization-oriented fusion.

4.1 *Experiment 1*

The data used for this experiment are an image scene on Taichung, Taiwan, taken by the IKONOS-2 satellite sensor in June 2001. The image size is 3000×3000 pixels. The Pan image and the corresponding RGB images are preprocessed by step 2 part 1, and displayed in Figs. 2(a) and 2(b), respectively. As shown in Fig. 2(b) for the test site, most of the area is covered by green vegetation. The fusion results achieved by nine fusion methods are displayed in Figs. 2(c)–2(k), respectively. Compared to the color of the original RGB image, obviously only the fused images generated by IHS, BT, and IHS-BT [Figs. 2(c), 2(d), and 2(e)] suffer from significant color distortion that has been efficiently mitigated in their generalized [Figs. 2(f), 2(g), and 2(h)] and spectral adjustment [Figs. 2(i), 2(j), and 2(k)] versions by introducing the NIR band into I.

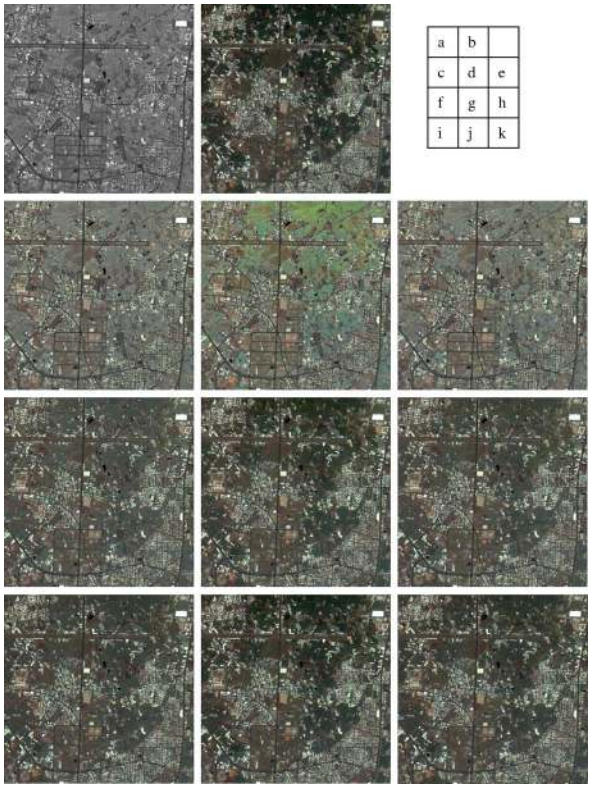

Fig. 2 A subsection of Taichung, Taiwan: (a) the output 8-bit Pan image by applying step 2 part 1; and (b) the output 8-bit RGB image by applying step 2 part 1. The fused images by (c) IHS, (d) BT, (e) IHS- BT, (f) GIHS, (g) GBT, (h) GIHS- BT, (i) SA-IHS, (j) SA-BT, and (k) SA-IHS- BT.

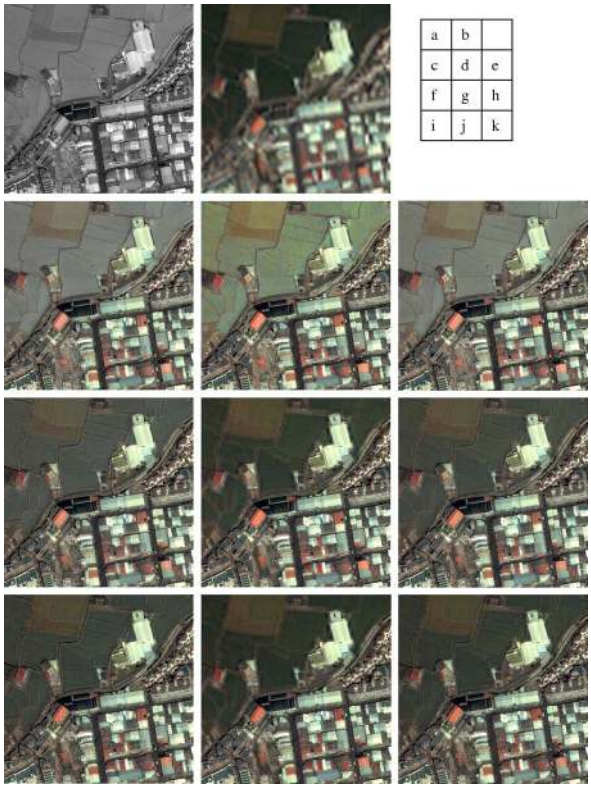

Fig. 3 The corresponding small chips with original resolution cut from Fig. 2.

The corresponding correlation coefficients for all nine image fusion methods are listed in Table 1. The correlation coefficients of those metrics are consistent with the results produced by visual evaluation. For clearer inspection, the corresponding small chips with original resolution cut from Fig. 2 are shown in Fig. 3. It can be easily seen that the fused images generated by the nine fusion methods, except for the green vegetation regions, demonstrate that their colors remain almost unchanged for all objects in the images, such as buildings, roads, and soil regions. In terms of spatial details, all spatial features in the Pan image are also perfectly integrated into the fused images. Compared to the colors of the green vegetation regions, Figs. 3(c), 3(d), and 3(e) reveal that the fused image generated by IHS is really saturation compressed, while saturation stretch is produced by BT. In line with our theoretical expectations, IHS-BT can be applied to effectively balance the saturation changes between IHS and BT.

Comparing GIHS, GBT, and GIHS-BT against SA-IHS, SA-BT, and SA-IHS-BT [Figs. 3(f), 3(g), and 3(h) versus 3(i), 3(j), and 3(k)] for spectral information preserving, the spectral adjustment versions outperform the generalized versions. Among those three spectral adjustment versions, SA-BT preserves the best spectral information and SA-IHS provides the most spatial details. For the purpose of classification-oriented fusion, the proposed SA-IHS-BT is a feasible approach by combining the merits of SA-BT and SA-IHS.

4.2 *Experiment 2*

The test image used in this experiment is a scene on Taipei, Taiwan, taken by the QuickBird satellite in April 2003. The

Table 1 Correlation coefficients associated with the nine fused images in Fig. 2.

	IHS	BT	IHS-BT	GIHS	GBT	GIHS-BT	SA-IHS	SA-BT	SA-IHS-BT
R	0.625	0.646	0.629	0.847	0.914	0.897	0.887	0.928	0.908
G	0.670	0.556	0.649	0.865	0.914	0.887	0.901	0.929	0.915
B	0.537	0.643	0.591	0.809	0.913	0.860	0.861	0.927	0.901
Pan	0.997	0.991	0.998	0.920	0.838	0.892	0.876	0.812	0.850

Fig. 4 A subsection of Taipei, Taiwan: (a) the output 8-bit Pan image by applying step 2 part 1; and (b) the output 8-bit RGB image by applying step 2 part 1. The fused images by (c) IHS, (d) BT, (e) IHS-BT, (f) GIHS, (g) GBT, (h) GIHS-BT, (i) SA-IHS, (j) SA-BT, and (k) SA-IHS-BT.

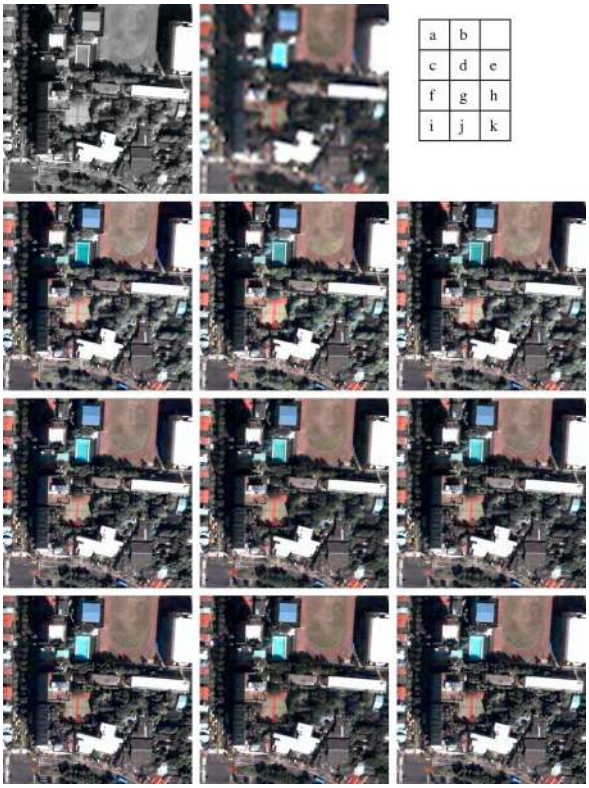

Fig. 5 The corresponding small chips with original resolution cut from Fig. 4.

size of the Pan image and the corresponding RGB images are 3000×3000 pixels and they are also preprocessed by step 2 part 1. Those images are displayed in Figs. 4(a) and 4(b), respectively. The fused QuickBird images achieved by nine fusion methods are individually shown in Figs. 4(c)–4(k). Those figures display the same results corresponding to Figs. 2(c)–2(k). Only the fusion results generated by IHS, BT, and IHS-BT exhibit unsatisfied spectral similarity on green vegetated areas, and their generalized and spectral adjustment versions can upgrade the color quality. Again, the corresponding correlation coefficients for all nine image fusion methods are listed in Table 2. For further comparison, the corresponding small chips with original resolution cut from Fig. 4 are shown in Fig. 5. As can be seen, the BTR response appeared on white roofs and the spatial details under the shadow of buildings are lost. To preserve most spectral and spatial information of the original 11-bit images with high visual quality, the BTR response remains an unavoidable problem.

According to the results shown in Figs. 5(c) through 5(k), again, SA-BT preserves the best spectral response and SA-IHS achieves the most spatial information. SA-IHS-BT provides the best tradeoff between spectral and spatial details. We need to specially add that all nine fusion methods can keep complete spatial features of the Pan image, but some details in the darker green vegetated areas are distorted. The fused image generated by SA-BT reveals that to preserve more spectral information in those areas results in more disappeared spatial details. Due to the scene-to-scene variations, the SA-IHS-BT with the saturation adjustment capability is an effective fusion technique for various areas.

Table 2 Correlation coefficients associated with the nine fused images in Fig. 4.

	IHS	BT	IHS-BT	GIHS	GBT	GIHS-BT	SA-IHS	SA-BT	SA-IHS-BT
R	0.773	0.770	0.771	0.871	0.896	0.880	0.893	0.908	0.899
G	0.744	0.717	0.739	0.851	0.885	0.864	0.877	0.901	0.887
B	0.719	0.750	0.735	0.840	0.882	0.856	0.871	0.897	0.882
Pan	0.999	0.999	0.999	0.967	0.931	0.957	0.939	0.905	0.929

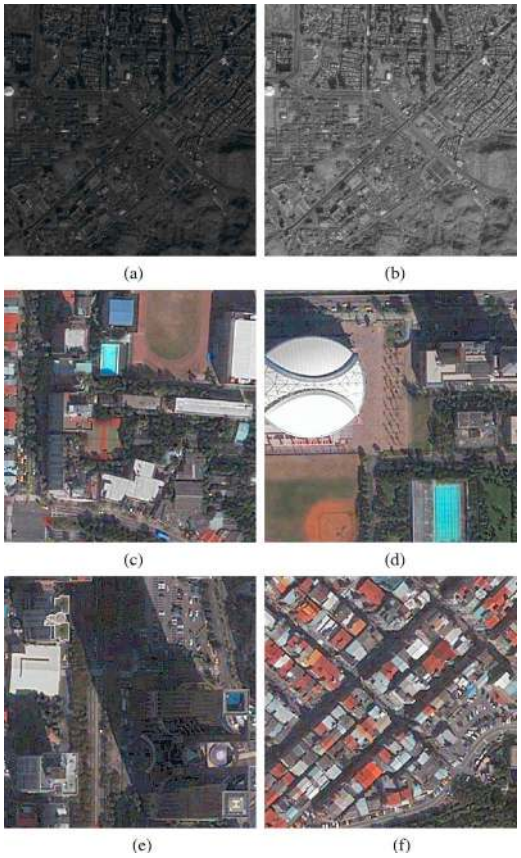

Fig. 6 (a) The output 8-bit Pan image by applying linear stretching; (b) the output image by applying step 2 part 1; and (c) through (f) small chips cut from the fused image.

4.3 *Experiment 3*

The purpose of this experiment is to verify that the proposed procedure can effectively reduce the BTR response and provide a good visualization-oriented fusion. In this experiment, we use the same QuickBird images in *Experiment 2* in Sec. 4.2. Figure 6(a) displays the 8-bit version of the Pan image after applying linear stretching to the original 11-bit image. Figure 6(b) is then generated by step 2 part 2. By comparing these two images, the image in Fig. 6(a) displays low contrast and its overall average brightness level is too dark for visualizing, while the image in Fig. 6(b) provides a good dynamic range compression. For comparison purposes, four small chips are cut from the fused image. They are displayed in Figs. 6(c)–6(f), and the BTR response that appeared on white roofs of Fig. 5 is obviously reduced. These chip images show that their colors remain almost unchanged for all objects in the image. The spatial details are, however, significantly increased. Even the lanes in a swimming pool [Fig. 6(d)] and the spatial details under the shadow of buildings and trees can be clearly recognized.

5 Conclusions

With the increasing use of high-resolution IKONOS/QuickBird images, it becomes essential to exploit techniques that are capable of quickly merging a huge amount of data while simultaneously preserving the most information from the original 11-bit Pan/MS images. For classification- and visualization-oriented fusion, the required techniques are different. To cope with this problem, a novel approach, the adjustable IHS-BT fusion technique, is developed for the IKONOS/QuickBird image fusion. By combining two simple DRA methods, the proposed fusion procedure can produce a high-quality fused image for different applications. The annoying BTR problem is also mitigated. Meanwhile, further experimental results using different IKONOS/QuickBird data have also reached similar conclusions.

Acknowledgments

The authors would like to thank RITI Technology, Incorporated, for providing Quickbird imagery. RITI is an agent of DigitalGlobe Company in Taiwan. The authors also thank the Space Imaging Company for providing IKONOS images. Finally, we would like to thank the National Science Council of the Republic of China for financially supporting this work under contract number NSC93-2623-7-014-016.

References

1. C. Pohl and J. L. Van Genderen, "Multisensor image fusion in remote sensing: Concepts, methods and applications," *Int. J. Remote Sens.* **19**, 823-854 (1998).
2. T. Ranchin and L. Wald, "Fusion of high spatial and spectral resolution images: The ARSIS concept and its implementation," *Photogramm. Eng. Remote Sens.* **66**, 49-61 (2000).
3. N. Jorge, O. Xavier, F. Octavi, P. Albert, P. Vicenc, and A. Roman, "Multiresolution-based imaged fusion with additive wavelet decomposition," *IEEE Trans. Geosci. Remote Sens.* **GE-37**, 1204-1211 (1999).
4. Y. Zhang, "Understanding image fusion," *Photogramm. Eng. Remote Sens.* **70**(6), 657-661 (2004).
5. T. M. Tu, S. C. Su, H. C. Shyu, and P. S. Huang, "A new look at IHS-like image fusion methods," *Info. Fusion* **2**, 177-186 (2001).
6. B. Aiazzi, L. Alparone, S. Baronti, and A. Garzelli, "Context-driven fusion of high spatial and spectral resolution images based on oversampled multiresolution analysis," *IEEE Trans. Geosci. Remote Sens.* **GE-40**, 2300-2312 (2003).
7. Y. Su, P. S. Huang, C. F. Lin, and T. M. Tu, "An approach to maximize increased details and minimize color distortion for IKONOS/QuickBird Image fusion," *Opt. Eng.* **43**, 3029-3037 (2004).
8. T. M. Tu, P. S. Huang, C. L. Hung, and C. P. Chang, "A fast intensity-hue-saturation fusion technique with spectral adjustment for IKONOS imagery," *IEEE Trans. Geosci. Remote Sens.* **GE-1**, 309-312 (2004).
9. J. G. Liu, "Smoothing filter-based intensity modulation: A spectral preserve image fusion technique for improving spatial details," *Int. J. Remote Sens.* **21**, 3461-3472 (2000).
10. *Geomaticas 9 User Manual*, PCI Geomatics Enterprises Inc., Richmond Hill, Ontario (2003).
11. *ENVI 4.1 User's Guide*, Research Systems Inc., Boulder, CO (2004).
12. *ERDAS IMAGINE 8.7 User's Guide*, Leica Geosystems GIS and Mapping Inc., Norcross, GA (2004).
13. Y. Zhang, "Problems in the fusion of commercial high-resolution satellite images as well as Landsat 7 images and initial solutions," *Geospatial Theory, Process. Appl. Proc. ISPRS Commission IV Symp.*, pp. 9-12 (2002).
14. D. C. He, L. Wang, and M. Amani, "A new technique for multiresolution image fusion," *IEEE Intl. Geosci. Remote Sensing Symp.* **7**, 4901-4904 (2004).
15. *HighView 1.5*, Geosage Inc., Australia (2004), See http://www.geosage.com/.
16. K. G. Nikolakopoulos, "Comparison of four different fusion techniques for IKONOS data," *IEEE Intl. Geosci. Remote Sensing Symp.* **4**, 2534-2537 (2004).
17. O. Rick, "Eye on quality—To DRA or not to DRA," *Imaging Notes* **5**, (2000), See http://www.imagingnotes.com/sepoct00/.
18. O. Rick, "Eye on quality—High-resolution color expectations," *Imaging Notes* **6**, (2000), See http://www.imagingnotes.com/novdec00/.
19. O. Rick, "Eye on quality—Clarity expectations for high-resolution satellite imagery," *Imaging Notes* **5**, (2001), See http://www.imagingnotes.com/mayjun01/.
20. K. A. Gerald, "Eye on quality—Beware of technological limitations,"

Imaging Notes **6**, (2002), See http://www.imagingnotes.com/novdec02/.
21. K. A. Gerald, "Eye on quality—points of view," *Imaging Notes* **18**(1), 2003, See http://www.imagingnotes.com/winter03/.
22. R. S. Ledley, M. Buas, and T. J. Golab, "Fundamentals of true-color image processing," *Proc. Int. Conf. Patt. Recog.* **1**, 791-795(1990).

Te-Ming Tu received his BSEE degree from the Chung Cheng Institute of Technology in 1986, his MSEE degree from the National Sun Yat-Sen University in 1991, and his PhD degree in electrical engineering from the National Cheng Kung University, in 1996. He was a teaching assistant from 1986 to 1989, an instructor from 1991 to 1993, and is currently a professor in the Department of Electrical Engineering, Chung Cheng Institute of Technology. His current research interests include multispectral/hyperspectral remote sensing, medical imaging, independent component analysis, and statistical pattern recognition.

Yuh-Chi Lee is currently an officer in Formosa Remote Sensing Center (FRSC) of Taiwan. He has been with the FRSC since 2001, working on image reception and processing. He was a staff member at the Data Processing Center of the Communication Research Laboratory of Taiwan from 1986 to 2000. He received his BS degree from Chung Cheng Institute of Technology in Taiwan in 1986 and his MS degree in computer science from University of Southern California, in 1996.

Chien-Ping Chang received his BS degree in electrical engineering from the Chung Cheng Institute of Technology in 1986, and his PhD degree in computer and information science from the National Chiao Tung University, Taiwan, in 1998. He is currently an associate professor in the Department of Electrical Engineering, Chung Cheng Institute of Technology, Taiwan. His research interests include parallel computing, interconnection networks, graph theory, image processing, and data hiding.

Ping Sheng Huang received his BSEE degree from the Chung Cheng Institute of Technology in 1985, his MS degree in computer science from University of Southern California in 1990, and his PhD degree in electronics and computer science from University of Southampton, United Kingdom, in 1999. Currently he is an associate professor in the Department of Electrical Engineering, Chung Cheng Institute of Technology. His research interests include digital image processing, biometric identification, and statistical pattern recognition.